Cation clustering in lithium silicate glasses: Quantitative description by solid-state NMR and molecular dynamics simulations

Ulrike Voigt, Heiko Lammert, Hellmut Eckert, and Andreas Heuer
Institut für Physikalische Chemie, Westfälische Wilhelms-Universität Münster, Corrensstrasse 30, D 48149 Münster, Germany
(Received 18 March 2005; revised manuscript received 27 June 2005; published 19 August 2005)

The local structural environment and the spatial distribution of the lithium ions in lithium silicate glasses with composition $(Li_2O)_x(SiO_2)_{1-x}(0<x\leqslant 0.40)$ is studied by nuclear magnetic resonance (NMR) and molecular dynamics (MD) simulation experiments. Site resolved $^{29}Si\{^7Li\}$ rotational echo double resonance (REDOR) studies reveal that the ^7Li dipolar fields measured at the $Q^{(3)}$ sites are significantly stronger than those at the $Q^{(4)}$ sites, and are almost independent of composition, implying a significant amount of cation clustering. For glasses with low lithia contents ($x=0.10$ and 0.17) these conclusions are qualitatively confirmed by molecular dynamics simulations and are consistent with the well-known tendency of such glasses to phase separate. Based on the combined interpretation of dipolar second moments $M_2(^{29}Si\text{-}^7Li)$ extracted from REDOR and partial pair correlation functions $g_{SiLi}(r)$ determined by MD simulation, a structural model for the lithia-enriched domains is proposed: each $Q^{(3)}$ unit is surrounded by approximately three lithium ions at an average distance of 320 pm, whereas the $Q^{(4)}$ units are much more remote from lithium. Detailed quantitative comparisons indicate that the clustering tendency suggested by MD is generally less pronounced than that indicated by the NMR results, and a significant structural difference is observed for $(Li_2O)_{0.33}(SiO_2)_{0.67}$ glass. Most likely, these discrepancies are consequences of the large difference in implicit cooling rates in the laboratory and the computer experiments, resulting in significantly different glass transition temperatures.

DOI: 10.1103/PhysRevB.72.064207 PACS number(s): 61.43.Fs, 76.60.Lz, 82.56.Ub, 61.43.Bn

I. INTRODUCTION

The structural properties of the mobile ions in ion conducting glasses have been the subject of considerable research activity during the past decade. Detailed anwers to questions on the local oxygen environment and the overall distribution of the mobile alkali metal ions in space may provide fundamental insights towards an improved understanding of cation transport in glasses. In particular binary alkali silicate glasses have been studied in considerable detail, using extended x-ray absorption fine structure (EXAFS),[1,2] nuclear magnetic resonance (NMR),[3–5] and diffraction methods.[6–8] In the regions of relatively low alkali oxide contents (<33 mol %) these studies have lent strong support to the "modified random network model" (MRN) in which the modifier cations are viewed to be concentrated in cluster regions and coordinated primarily by nonbridging oxygen atoms.[1,2] The percolation of such clusters may lead to the formation of "ion conducting channels" at higher concentrations. The general results of these studies are consistent with the tendencies of alkali silicate glasses to phase separate, which has been well documented by experimental results and discussed on a thermodynamic basis.[10–16] Specifically, in the Li_2O-SiO_2 system the liquidus curve reveals strongly nonideal mixing behavior at low lithia concentrations, and a subliquidus metastable liquid immiscibility region spanning the range $0<x<0.33$ has been identified; similar effects are also visible in sodium silicate glasses.[14,15] Consistent with this nonideal mixing behavior, molecular dynamics simulations on alkali silicate glasses have generally suggested that the ions are distributed inhomogeneously and that cation motion occurs in channel-like domains.[17–27] Most of the previous experimental and theoretical investigations have focused on the system Na_2O-SiO_2, although results on lithium silicate glasses have also been published. From comparison of experimental with simulated data for the scattering function as well as for activation energies of transport quantities nice agreement between experiment and simulation could be observed.[28] Furthermore there is ample indirect spectroscopic evidence that the extent of cation clustering in silicate glasses is strongly influenced by the cation type.[29–34]

For enabling comparisons between different glass systems, it would thus be of great interest to characterize cation clustering tendencies in glasses by means of suitable quantitative criteria. A particularly valuable observable in this respect is the magnetic dipole-dipole coupling, since it can be measured with high precision using advanced solid state NMR methodology,[35] and calculated straightforwardly from the internuclear distance distributions of any structural scenario.[36] To gain more insight into the numbers of interacting spins and their corresponding distances, however, it is essential to combine this experimental NMR analysis with state-of-the-art molecular dynamics (MD) simulations. Indeed, the complementarity of NMR and MD experiments has already proven useful for studying other structural aspects (network connectivity) in silicate glasses.[6] In this contribution we will present the combined NMR and MD analysis of magnetic dipole-dipole interactions, resulting in a quantitative description of cation clustering in lithium silicate glasses.

II. FUNDAMENTAL CONCEPTS AND METHODOLOGY

The local network structure of lithium silicate glasses is well understood on the basis of numerous spectroscopic techniques. Incorporation of lithium oxide into molten silica

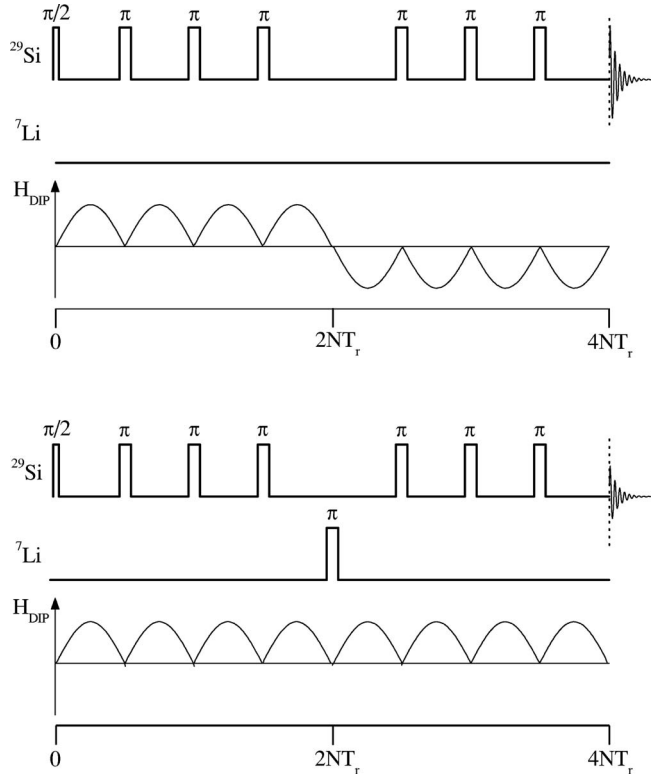

FIG. 1. REDOR pulse sequence used in the present study. Dipolar recoupling is accomplished by the ^{7}Li π pulse in the middle of the rotor period.

results in network depolymerization associated with the conversion of Si-O-Si linkages into negatively charged Si-O$^-$ groups, which compensate the positive charge of the nearby Li^+ ions. Overall five different types of silicon species are possible, which are denoted $Q^{(n)}(0 \leqslant n \leqslant 4)$, n being the number of bridging oxygen atoms per silicon atom. These $Q^{(n)}$ species can be spectroscopically resolved and quantitatively determined by ^{29}Si magic-angle spinning (MAS) NMR spectroscopy.[29–34]

In the present study, we seek information on cation clustering in lithium silicate glasses of composition $(Li_2O)_x(SiO_2)_{1-x}$ by studying the magnetic dipole-dipole interactions between the ^{7}Li spins and the various $Q^{(n)}$ species in the network in a site selective fashion. The principle of local charge minimization implies that any clustering involving the lithium ions must be accompanied by an equal extent of clustering involving the charge compensating nonbridging oxygen atoms.[37] In the region of relatively low lithia contents ($x \leqslant 0.33$), where the network structure is dominated by $Q^{(4)}$ and $Q^{(3)}$ units, any cation clustering will then produce significantly stronger ^{29}Si-^{7}Li magnetic dipolar interactions for the negatively charged $Q^{(3)}$ groups than for the electrostatically neutral $Q^{(4)}$ units. The corresponding dipolar coupling strengths can be measured in a site-selective fashion by rotational echo double resonance (REDOR) NMR.[38,39] Figure 1 shows the pulse sequence used in the present study. A normalized difference signal $\Delta S/S_0 = (S_0\text{-}S)/S_0$ is measured in the absence (intensity S_0) and the presence (intensity S) of the dipolar interactions of the observed nuclei S with the second nuclear species I. Determination of $\Delta S/S_0$ under systematic variation of the number of rotor cycles N affords the so-called REDOR curve, in which the data are plotted as a function of dipolar evolution time $N\,T_r$ (T_r being the duration of one rotor period). For isolated spin-1/2-pairs these curves possess a universal shape, allowing the straightforward determination of the magnetic dipole coupling constant.[38,39] In contrast, the analysis of REDOR curves in inorganic glasses is complicated by multispin interactions, distance distributions, and interference by nuclear electric quadrupolar couplings. We have previously shown that these problems can be overcome by detailed simulation and model compound work, developing this method into an experimental tool affording a site-resolved measurement of heteronuclear dipolar coupling in glasses.[40–42] Specifically, we have shown that for the initial regime ($\Delta S/S_0 \leqslant 0.2$) the REDOR curve is well approximated by a parabola, the curvature of which corresponds to the van-Vleck second moment $M_2^{I\text{-}S}$:

$$\frac{\Delta S}{S_0} = \frac{4}{3\pi^2}(NT_r)^2 M_2^{I\text{-}S}. \tag{1}$$

This quantity is particularly well suited for characterizing average dipole-dipole coupling strengths in disordered materials, where the order and geometry of the spin system is unknown, and possibly ill defined. In cases where the dipolar dephasing of the observed spins occurs in the local field of $I > 1/2$ nuclei such as ^{7}Li($I=3/2$) several complications enter. First of all, the different possible Zeeman states m_I for the I nuclei differ in the respective sizes of their z components and, hence, generate dipolar fields of different magnitudes at the observed spins.[43,44] Second for larger C_Q values, the anisotropic broadening of the $|\pm 1/2\rangle \leftrightarrow |\pm 3/2\rangle$ "satellite transitions" produces large resonance offsets, which reduce the efficiency of the π pulses to cause population inversion. For sufficiently strong quadrupolar interactions, only the central $|1/2\rangle \leftrightarrow |-1/2\rangle$ coherences will be affected. In this limiting case only those S spins that are coupled to I nuclei in Zeeman states with $|m_I| = 1/2$ are expected to yield a REDOR response. Detailed simulations of this situation have led to the conclusion that it is desirable in such cases to mimimize the number of π pulses applied to the quadrupolar nuclei, making the REDOR sequence of Fig. 1 the method of choice. As we have previously shown, the initial curvature analysis discussed above can be extended to systems containing $I=3/2$ nuclei by using the expression

$$\frac{\Delta S}{S_0} = \frac{1}{15\pi^2}(2 + 18f_1)(NT_r)^2 M_2^{I\text{-}S}, \tag{2}$$

where the efficiency factor $f_1 (0 < f_1 < 1)$ accounts for the extent to which the dipolar coupling of S spins to I spins in their outer Zeeman states still influences the REDOR response. Again, Eq. (2) is valid for the initial regime ($0 \leqslant \Delta S/S_0 \leqslant 0.2$) only.[42]

The whole data analysis procedure can thus be summarized as follows. Based on a nuclear electric quadrupolar coupling constant known from experiment, a universal REDOR curve is computed (using the SIMPSON code,[45]) using

explicitly those experimental conditions under which the REDOR data were taken. This simulation curve is fitted to a parabola [Eq. (2)], resulting in the appropriate f_1 value, which is then applicable for the analysis of the experimental data set. Using the f_1 value determined in this fashion, the experimental data set is fitted to Eq. (2), resulting in an experimental $M_2^{I\text{-}S}$ value. This value can then be compared with a second moment calculation from the van Vleck formula[36] for testing hypothetical structural scenarios

$$M_2 = \left(\frac{\mu_0}{4\pi}\right)^2 \frac{4}{15} S(S+1)\hbar^2 \gamma_S^2 \gamma_I^2 \sum_S r_{IS}^{-6}. \quad (3)$$

In Eq. (3) γ_I and γ_S are the gyromagnetic ratios of the nuclei I and S involved, and r_{IS} are internuclear distances. In the present study, we will use this approach to analyze the dipolar field created by the ^{7}Li nuclei at the ^{29}Si sites, using ^{29}Si{^{7}Li} REDOR spectroscopy. For example, the Li_2O-concentration dependence of M_2, i.e., $M_2(x)$ forms a basis for distinguishing between different lithium ion distribution scenarios. In case of vanishing x dependence, i.e., $M_2(x) \propto x^0$, the respective silicon sites possess a lithium environment which is independent of the total lithium concentration. Due to the strong dependence of the dipolar coupling on distance this conclusion mainly holds for the nearest neighbor (nn) shell. Chemically this corresponds to a well-defined local structure which is preferred due to energetic reasons. In contrast, a linear dependence $M_2(x) \propto x$ indicates a statistical distribution scenario. Finally, the x dependence of $M_2(x)$ may be even stronger than linear. The standard scenario for this case is the so-called homogeneous limit in which the atoms try to maximize their respective distances, leading to $M_2(x) \propto x^2$.[46] A different scenario will be presented further below to rationalize the second moments for the $Q^{(4)}$ species.

A particular goal of the present study is the comparison of the experimental data with predictions made by MD simulations, which produce the full information about the microscopic structure. From the simulated structures the values of M_2 can be obtained according to Eq. (3). Beyond this r weighted average of the respective distances it is also possible to obtain the full distribution of distances. The standard quantity for this purpose is the partial pair correlation function $g_{ij}(r)$. It is a measure for the probability that atoms of species i are surrounded by atoms of species j at a distance of r. Note that $g_{ij}(r)$ is normalized such that $g_{ij}(r \to \infty) = 1$. For the simulations $g_{Li,Li}(r)$ and $g_{Si,Li}(r)$ will be analyzed. In analogy to the experiment $g_{Si,Li}(r)$ is individually determined for the different $Q^{(n)}$ units. We note in passing that the relation between the second moment and the pair correlation function can be written as

$$M_2 = c \int dr \frac{4\pi r^2 g_{Si,Li}(r)}{r^6} \frac{N_{Li}}{V} \quad (4)$$

with the constant $c = 3.4 \times 10^9$ Å$^6/s^2$. The ratio N_{Li}/V denotes the particle density of the lithium ions. Analysis of $g_{ij}(r)$ (or of correlation functions derived from it) is, of course, much more informative than the second moment alone because direct information about the coodination number, the typical distances of the nearest neighbors and the properties beyond the nn shell is accessible.

An analogous discussion of different scenarios can be based on the partial pair correlation function $g_{ij}(r)$, or the corresponding scaled pair correlation function defined by

$$f_{ij}(r) = g_{ij}(r)x. \quad (5)$$

Again, it is instructive to study the concentration dependence, by considering the intensity of the nn peaks in $f_{ij}(r)$ and $g_{ij}(r)$. Concentration independence of the nn-peak intensity in $g_{ij}(r)$ implies that the distribution of ions around the central atom is purely statistical, i.e., the number of ions in the nn shell is proportional to the density of ions [$M_2(x) \propto x$]. In contrast, concentration independence of the nn-peak intensity in $f_{ij}(r)$ suggests that the lithium distribution in the nn shell is independent of concentration [$M_2(x) \propto x^0$].

There is one major problem, however, when comparing experiments and simulations on this detailed level. Even on modern computers with optimized software it is hard to extend the time scale of 100 ns for individual simulation runs. This inherent limitation implies that very high cooling rates have to be applied to generate structures below the glass transition temperatures. Typical cooling rates are at least 10^{10} K/s, to be compared with typical experimental cooling rates of $1–10^2$ K/s. As a consequence specific structural features such as clustering phenomena, suggested by thermodynamics and correspondingly observed experimentally, may not be fully realized due to the kinetic limitations in simulations. The same holds for the distribution of $Q^{(n)}$ units.

III. EXPERIMENT

A. Sample preparation and characterization

Binary glasses in the system $(Li_2O)_x$-$(SiO_2)_{1-x}$ ($0.1 \leqslant x \leqslant 0.40$) were prepared by heating mixtures of Li_2CO_3, (Merck 99.9%), SiO_2 (Fluka, p.a. $\geqslant$ 230 mesh) in platinum crucibles for 2–3 h at temperatures between 1300 and 1650 °C, followed by quenching in liquid nitrogen. To accelerate ^{29}Si NMR spin-lattice relaxation, the batches included 0.1 mol % $MnCO_3$ (Riedel de Haen, p.a.), resulting in a doping of the glass with paramagnetic Mn^{2+} ions. Glass transition temperatures (onset points), measured on a Netzsch DSC 200 differential scanning calorimeter, were found in good agreement with reported values in the literature in the absence of doping. Based on this result (as well as the structural data from MAS-NMR discussed below) we consider the influence of Mn^{2+} on the network structure organization of these glasses to be minimal.

B. NMR experiments

Standard ^{29}Si MAS-NMR spectra were recorded at 59.62 MHz using a Bruker CXP 300 NMR spectrometer equipped with a TECMAG pulse controller and a 7 mm MAS probe operated at a rotor frequency of 4 kHz. Typically 1000–1600 scans were signal averaged with 45° pulses of 4–6 μs length and relaxation delays of 30–60 s. Chemical shifts were ex-

TABLE I. Compositions and standard characterization details of the samples studied.

x	T_g (K) (±5 K)	$Q^{(2)}$ (%)	$Q^{(3)}$ (%)	$Q^{(4)}$ (%)	^{7}Li: δ_{iso} (ppm) (±0.05)	^{7}Li: C_Q (kHz) (±20)	π pulse length (μs) for ^{7}Li	$f_1[Q^{(3)}]$	$f_1[Q^{(4)}]$
0.1	736	4	24	73	0.14	320	11.8	0.3285	0.3945
0.15	739	8	37	55	0.18	320	11.6	0.3288	0.3368
0.20	740	7	50	43	0.17	340	8.3	0.4939	0.4939
0.25	735	7	58	35			8.2	0.4952	0.5462
0.33	728	24	55	21	0.25	340	8.0	0.4960	
0.4	721	41	55	4	0.40	340	7.8	0.4965	
Li_2SiO_3						200	7.3	0.7306	

ternally referenced against a tetramethylsilane standard. Spectral deconvolution carried out with the DMFIT program[47] resulted in $Q^{(n)}$ distributions consistent with the sample compositions. ^{7}Li MAS-NMR spectra were measured at 194.31 MHz using a Bruker DSX-500 NMR spectrometer, and a 4 mm MAS probe operated at a rotor frequency of 10 kHz. Chemical shifts are externally referenced to a 1 M aqueous solution of LiCl. To estimate the magnitude of the quadrupolar coupling constant, the spinning sideband manifold associated with the $|\pm 1/2\rangle \leftrightarrow |\pm 3/2\rangle$ satellite transitions was recorded, using 90° pulses of 2.8 μs length and a recycle delay of 2s. ^{29}Si{^{7}Li} REDOR experiments were conducted on the same spectrometer using a MAS probe double-tuned for ^{29}Si (99.33 MHz) and ^{7}Li (194.32 MHz). The pulse sequence of Fig. 1 was used, employing ^{29}Si-180° pulse lengths between 6 and 13.5 μs, and ^{7}Li 180° pulse lengths between 7.3 and 11.8 μs (see Table I). The 180° pulses were optimized by maximizing the REDOR difference signal. To generate enough data points for the initial curvature analysis, the measurements were conducted at three MAS rotor frequencies of 10, 12, and 14 kHz. Typically 100 scans were signal averaged at a recycle delay of 30 s. For each dipolar evolution time, the reference signal intensity S_0 and the REDOR intensity S were measured in direct succession; and the REDOR difference signal intensities determined via the DMFIT routine,[47] constraining all line shape parameters except for amplitude. Following each scan, a saturation comb was employed to restore a reproducible stationary magnetization. Simulations of the REDOR response were carried out with the SIMPSON code,[45] using exactly the same conditions as those employed in the experiments.

C. MD simulations

The potential energy of the lithium silicate system is chosen to be the sum of a Buckingham and a Coulomb pair potential

$$U_{ij}(r_{ij}) = q_i q_j/(4\pi\varepsilon_0 r_{ij}) - C_{ij}/r_{ij}^{\ 6} + A_{ij}\exp(-B_{ij}r_{ij}). \quad (6)$$

The indices i and j denote the species lithium, oxygen, and silicon, respectively. The potential parameters are listed in previous work by Banhatti and Heuer.[28] They are based on *ab initio* calculations by Habasaki.[48–50] Using the MOLDY software package, we have generated MD trajectories in the NVT ensemble, i.e., at constant volume. The length of the elementary time step was chosen to be 2 fs and periodic boundary conditions were used. $(Li_2O)_x$-$(SiO_2)_{1-x}$ glasses with $x=0.1$, $x=0.17$, and $x=0.33$ were simulated with system sizes of $N=1200$, $N=1206$, and $N=1215$, respectively. The densities were taken from experimental room temperature data.[51] We have performed long simulation runs above the glass transition temperature T_g to equilibrate the total system at the lowest possible temperature. The values of T_g obtained from equating the alpha relaxation time to 100 ns, i.e., the time scale of our simulations, are approximately 1250 K for $x \leqslant 0.17$ and 1100 K for $x=0.33$. For all temperatures below T_g the lithium subensemble can still equilibrate, whereas the network is basically frozen in, corresponding to the structure at T_g. Afterward we have recorded the partial pair correlation functions from simulations taking ~10 ns. While we report data for the lowest temperatures considered, $T=920$ K, $T=1125$ K, and $T=850$ K, for $x=0.1$, $x=0.17$, and $x=0.33$, respectively, the structural quantities were found to be basically temperature independent below T_g.

IV. RESULTS, DATA ANALYSIS AND INTERPRETATION

A. ^{29}Si{^{7}Li} REDOR of crystalline Li_2SiO_3

For validation, the ^{29}Si{^{7}Li} REDOR approach described above was applied to the model compound lithium metasilicate (see Fig. 2). For this compound, three crystal structure solutions are available in the literature,[52–54] from which $M_2(^{29}\text{Si-}^7\text{Li})$ values of 53.7×10^6 s^{-2}, 48.7×10^6 s^{-2}, and 47.8×10^6 s^{-2} are calculated via Eq. (3). We consider these differences insignificant in view of the statistical and systematic errors involved in the experimental M_2 measurement. For determining the scaling factor applicable to the experimental REDOR data, knowledge concerning the ^{7}Li quadrupolar coupling tensor is required. From the spinning sideband manifold associated with the satellite transitions of the ^{7}Li NMR signal (Fig. 3), we can estimate a nuclear electric quadrupole coupling constant $C_Q=200\pm10$ kHz. No reliable information on the electric field gradient asymmetry parameter is available, however, resulting in a minor uncertainty for the f_1 value. Based on SIMPSON simulations, we can de-

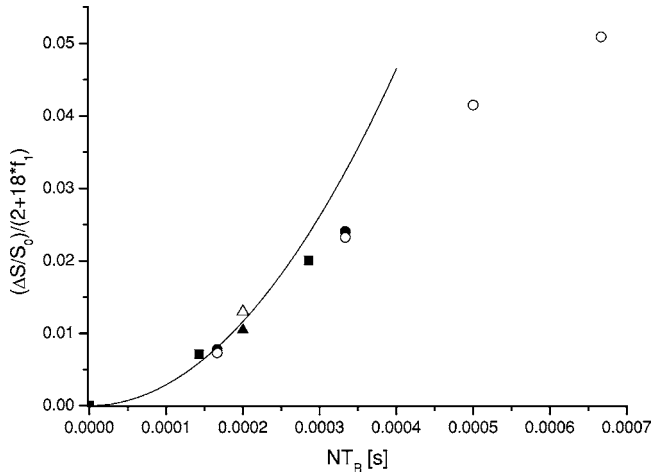

FIG. 2. ^{29}Si{^{7}Li} REDOR curve of crystalline Li_2SiO_3. Open and closed symbols originate from two independent experiments. For each data set, squares, circles, and triangles represent data obtained at spinning speeds of 14, 12, and 10 kHz, respectively. The solid curve denotes the parabolic fit to Eq. (2), corresponding to a second moment of 43×10^6 s^{-2}

duce $f_1=0.749$, 0.738, and 0.705 for $\eta=0$, 0.5, and 1, respectively. Using the average value $f_1=0.731$, we have analyzed the experimental REDOR curve over the data range $\Delta S/S_0 \leqslant 0.2$ in terms of Eq. (2). Figure 2 also includes data points obtained in a second separate run at different radio frequency field amplitude, where $f_1=0.635$ was obtained (open symbols), giving consistent results. The M_2 value determined from all of the data, $(43\pm10)\times10^6$ s^{-2}, is in reasonable agreement with the value predicted from the crystal structure. Unfortunately, the extremely long spin-lattice relaxation time of Li_2SiO_3 leads to rather low signal-to-noise ratio and, hence, a low-precision M_2 value. For the glasses, the situation is significantly improved because of more favorable relaxation characteristics.

B. ^{29}Si{^{7}Li} REDOR of Lithium Silicate glasses

Figure 4 displays the ^{29}Si MAS NMR spectra and a representative ^{7}Li MAS-NMR spectrum of the glasses. The ^{29}Si NMR spectra can be deconvoluted into Gaussian contributions assigned to $Q^{(4)}$, $Q^{(3)}$, and $Q^{(2)}$ units, with parameters in agreement with the literature.[29–34] The spectral deconvolution results and the relevant interaction parameters deduced from these spectra are summarized in Table I. The ^{7}Li NMR data are generally consistent with previous measurements,[55] however, they reveal more clearly that for $x\leqslant0.33$ the ^{7}Li chemical shifts are essentially independent of composition, suggesting that a constant lithium environment is produced at low concentrations. Also, the ^{7}Li nuclear electric quadrupolar coupling constants extracted from the satellite spinning sideband manifolds are found to be constant over the entire composition range. Based on these C_Q values, and the experimental REDOR conditions used, the applicable correction factors f_1 were determined by SIMPSON simulation for

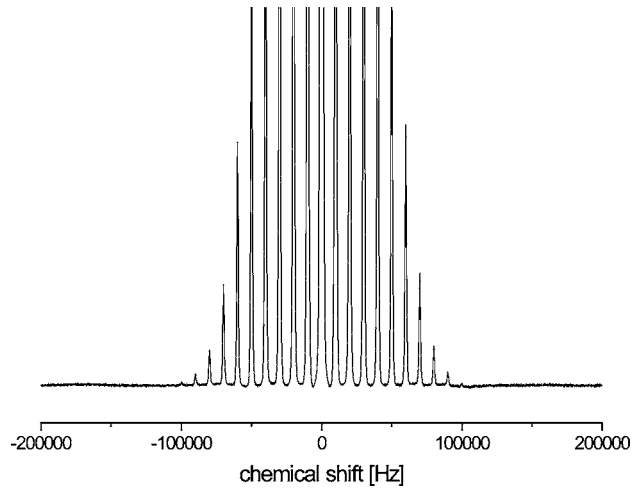

FIG. 3. ^{7}Li spinning sideband manifold for the model compound Li_2SiO_3.

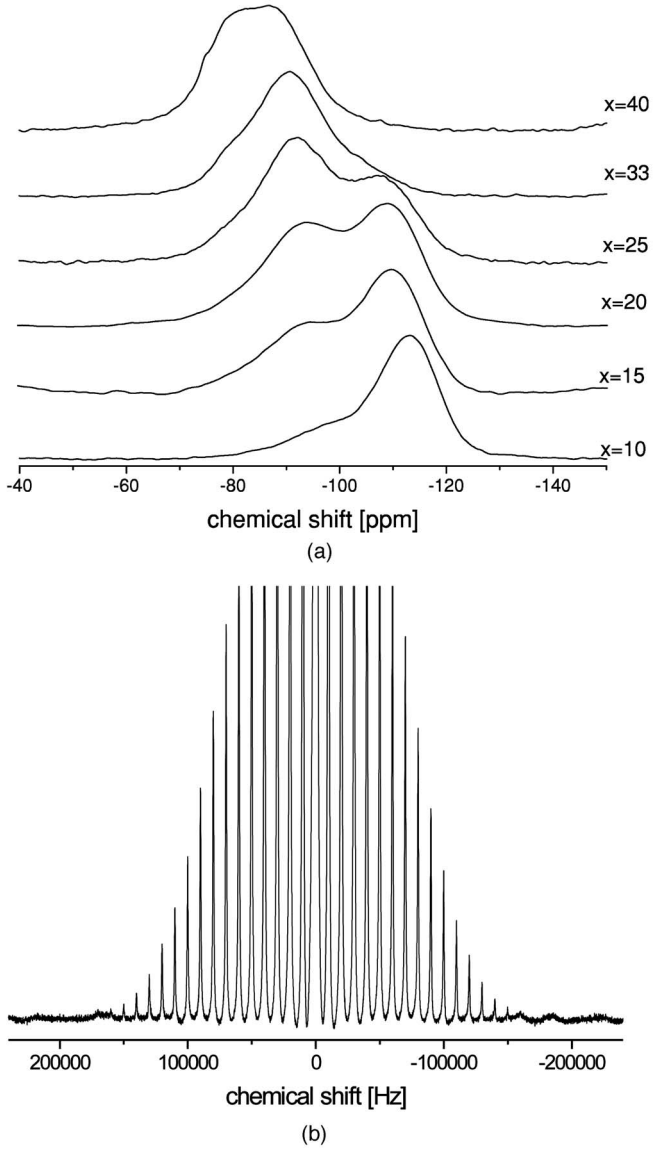

FIG. 4. Characterization of the lithium silicate glasses by standard MAS NMR. (a) ^{29}Si spectra as a function of composition x (mol % Li_2O). (b) ^{7}Li spinning sideband manifold in glass with $x=15$ mol % Li_2O.

each REDOR data set. The results are included in Table I, and represent again averages across the η range between zero and unity. Systematic simulations indicate further that even within the restricted $\Delta S/S_0 \leqslant 0.2$ data range the applicable f_1 value is not constant, but shows a non-negligible dependence on the actual $\Delta S/S_0$ data range used, since the parabolic approximation [Eq. (2)] is not perfect. This dependence, shown in Fig. 5, must also be taken into account here, as the experimental $\Delta S/S_0$ data ranges used for the parabolic analysis differ from sample to sample: while the REDOR data relating to the $Q^{(3)}$ species always cover the full $\Delta S/S_0 \leqslant 0.2$ data range, the data relating to the $Q^{(4)}$ species do not go beyond $\Delta S/S_0 = 0.1$ in most of the samples. For this reason, different f_1 values are generally applicable for the analysis of the experimental data relating to the $Q^{(3)}$ and the $Q^{(4)}$ units in a given REDOR data set.

Figures 6(a)–6(f) summarize the experimental REDOR curves, along with their corresponding parabolic fits, producing the experimental $M_2(^7\text{Li-}^{29}\text{Si})$ values listed in Table II. First of all, there is a one order of magnitude difference between the values measured for the $Q^{(3)}$ units and those measured for the $Q^{(4)}$ units, indicating that the latter are very remote from the network modifier species in all of the glasses with lithium oxide contents below 25 mol %. At the same time the $M_2(^7\text{Li-}^{29}\text{Si})$ values measured for the $Q^{(3)}$ units are nearly independent of composition in this concentration region. All of these results are consistent with microphase or nanophase segregation into a lithium silicate domain and a second silica-rich phase having very low lithium content. Furthermore, these results suggest that, regardless of the bulk composition, the Li/Si ratio of the lithium-rich domain and its structural organization remain more or less independent of x.

C. MD results

Table III summarizes the $Q^{(n)}$ distributions and the site selective $M_2(^{29}\text{Si-}^7\text{Li})$ values extracted from the MD simulations. In addition, we list average $Q^{(3)}$-Li distances as determined from the maximum observed in $g_{Si,Li}(r)$. Furthermore, Table III lists estimated coordination numbers CN for the $Q^{(3)}$ units with lithium, which are compared with predicted values for statistical distributions. The quantitative $Q^{(n)}$ distributions are generally in reasonable agreement with the experimental data and results published in the literature[29–33] and similar to previous simulation data for sodium siliate.[6] However, in contrast to the results of Ref. 6, no five-coordinate silicon species are observed in our simulations. To facilitate the comparison of MD and NMR results with respect to the issue of the silicon-lithium proximities and interactions, the MD results have been analyzed with respect to the following aspects.

1. *Different lithium environment for different $Q^{(n)}$ units*. The NMR experiments reveal that for each sample, $M_2(^7\text{Li-}^{29}\text{Si})$ increases in the order $Q^{(4)} > Q^{(3)} > Q^{(2)}$ suggesting that the number of nearby lithium ions increases in that order. This tendency is clearly reproduced in the computer simulations as shown in Fig. 7 where $g_{Li,Si}(r)$ is shown for different $Q^{(n)}$ units for $x=0.33$.

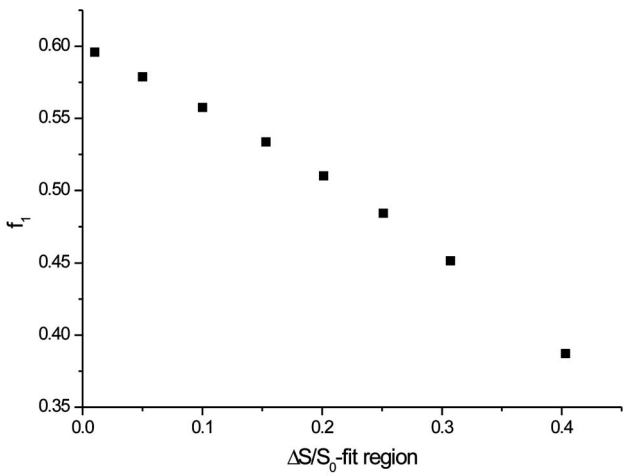

FIG. 5. Dependence of the calibration factor f_1 on the $\Delta S/S_0$ data range used in the parabolic analysis.

2. *Segregation of lithium*. In Fig. 8 we show $g_{Li,Li}(r)$ for three concentrations. Evidently, the nearest-neighbor peak increases with decreasing concentration. This shows that indeed there is clustering of lithium ions at lower concentrations. In the limit of full segregation one would have expected that the nn-peak height increases proportional to the inverse concentration which obviously is not the case. In agreement with expectation the very fast cooling process during computer simulations does not allow the system to find its segregated limit. A significant tendency towards this limit, however, can be observed

3. *Lithium environment of $Q^{(3)}$ units as a function of Li content*. One major result of the REDOR experiments is the observation that $M_2(^7\text{Li-}^{29}\text{Si})$ related to the $Q^{(3)}$ units is relatively constant, indicating a specific structural local organization independent of concentration. For $x=0.10$ and 0.17, this result is in excellent agreement with the MD simulation results. As shown in Table III, the M_2 values obtained from the computer simulations are found in quantitative agreement (within 15%) with the experimental data. For a better understanding it is instructive to analyse $f_{Si,Li}(r)$, shown in Fig. 9. As discussed above a constant second moment should show up as a concentration independence of $f_{Si,Li}(r)$ in the nn shell. Comparing $x=0.1$ and $x=0.17$ one indeed finds that $f_{Si,Li}(r)$ is rather similar in the nn shell. The behavior in the nn shell has to be compared with the behavior at larger distances where $f_{Si,Li}(r) \propto x$ as expected for the purely statistical case. Table III indicates further that for $x=0.10$ and 0.17 the average $Q^{(3)}$-Li coordination number is significantly higher than expected for a purely statistical distribution, whereas for $x=0.33$ the MD simulation produces the statistically expected result. As discussed further below, Tables II and III reveal significant discrepancies between the NMR and the MD results regarding both the M_2 values and the $Q^{(3)}$-Li coordination numbers in lithium disilicate glass.

4. *Lithium environment of $Q^{(4)}$ units as a function of Li content*. As shown in Table III, NMR and MD results produce significantly different conclusions concerning the lithium environment of the $Q^{(4)}$ units. The M_2 values determined from the simulation suggest that the $Q^{(4)}$-Li interac-

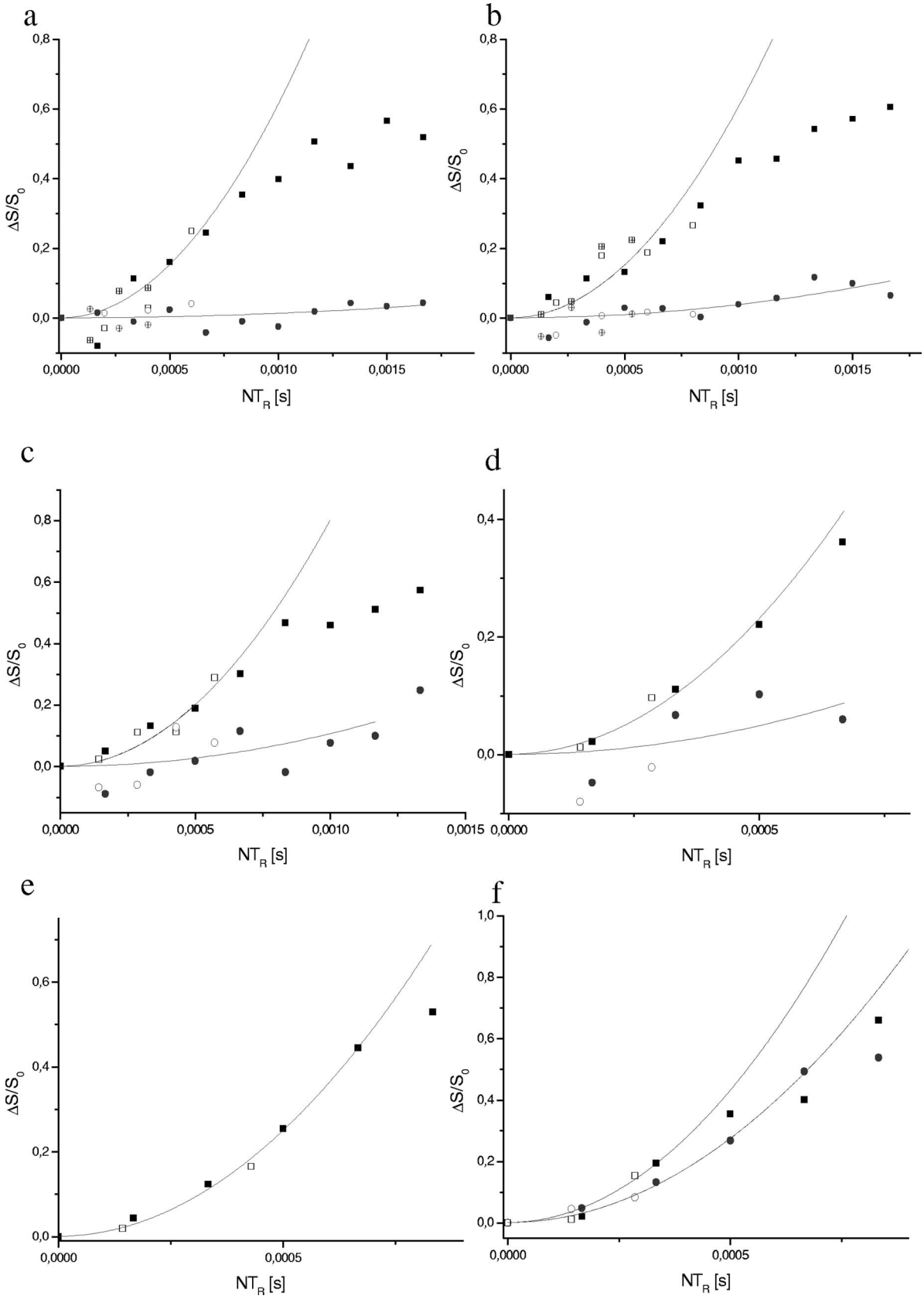

FIG. 6. ^{29}Si{^{7}Li} REDOR data of lithium silicate glasses containing as a function of lithium oxide concentration. The plots (a)–(f) correspond to lithia contents of 10, 15, 20, 25, 33, and 40 mol %. In parts a-e, squares denote data obtained at different spinning speeds for the $Q^{(3)}$ sites, circles denote data obtained at different spinning speeds for the $Q^{(4)}$ sites. In part *f*, squares denote data for the $Q^{(2)}$ sites and circles denote data for the $Q^{(3)}$ sites. Crossed, filled, and open symbols indicate data at spinning speeds of 14, 12, and 10 kHz, respectively.

TABLE II. ^{7}Li-^{29}Si-M_2 values determined for the resolved $Q^{(n)}$ species in the glasses under study. From the M_2 values relating to the $Q^{(3)}$ species, possible ranges of coordination numbers CN[$Q^{(3)}$-Li] have been derived, using the procedure outlined in the text. The error quoted for CN (±0.3) arises from the precision (±5pm) with which the maximum in g_{SiLi} is determined from the MD simulations. For the explanation regarding the upper and lower limits quoted, see text.

	$M_2[Q^{(4)}](\pm 10\%)$ (10^6 s^{-2})	$M_2[Q^{(3)}](\pm 10\%)$ (10^6 s^{-2})	$M_2[Q^{(2)}](\pm 10\%)$ (10^6 s^{-2})	CN[$Q^{(3)}$-Li] (±0.3)
$(Li_2O)_{10}(SiO_2)_{90}$	0.2	11.5		2.8–3.5
$(Li_2O)_{15}(SiO_2)_{85}$	0.7	11.3		2.9–3.6
$(Li_2O)_{20}(SiO_2)_{80}$	1.4	11.6		3.0–3.7
$(Li_2O)_{25}(SiO_2)_{75}$	2.4	12.5		3.0–3.7
$(Li_2O)_{33}(SiO_2)_{66}$		13.5		3.0–3.7
$(Li_2O)_{40}(SiO_2)_{60}$		14.8	23.3	3.2–4.0

tions are significantly stronger than indicated by the NMR data. Consistent with this discrepancy, different concentration dependences are observed. While the simulations show $M_2(x) \propto x$ and $f_{Si,Li}(r) \propto x$, as expected for a statistical distribution, the NMR experiments suggest $M_2 \propto x^2$. Possible mechanisms accounting for this superlinear concentration dependence will be discussed below.

V. DISCUSSION

A. Lithium cluster distance geometry from NMR and MD simulations

For the region of low lithia contents ($x \leqslant 0.17$) the NMR data and the MD simulations are in excellent conceptual agreement, favoring a structural description of lithium silicate glasses in terms of a clustering model. We can combine these results to reveal information about the structural organization of the lithium-rich nanophase. Based on the average $Q^{(3)}$-Li distances determined from the maxima in the $g_{SiLi}(r)$ curve (see Table III), we can estimate the number of Li nearest neighbors to a $Q^{(3)}$ silicon unit from the experimental M_2 values. For example, taking $r_{SiLi}=318\pm5$ pm as the relevant average $Q^{(3)}$-Li closest distance in the $x=0.1$ glass, each closest lithium neighbor would produce a contribution of $3.29\pm0.30\times10^6$ s^{-2} to M_2(^{7}Li-^{29}Si). Thus, the experimental M_2 value of 11.5×10^6 s^{-2} can be "translated" into an average $Q^{(3)}$-Li coordination number (CN) of 3.5 ± 0.3. For the other glasses, the relevant distances are: $r_{SiLi}=321\pm5$ pm ($x=0.15$ and 0.2), $r_{SiLi}=312\pm5$ pm ($x=0.33$ and 0.40), and $r_{SiLi}=316$ pm (interpolated value for $x=0.25$), resulting in the average coordination numbers listed in Table II. These should be considered upper-limit values, because our analysis neglects the fact that the experimentally measured M_2 values also include contributions from more remote lithium atoms. The systematic error arising from this simplification can be estimated from the structure of crystalline $Li_2Si_2O_5$. In this compound, each $Q^{(3)}$ unit is surrounded by five lithium neighbors, at distances 290.1, 298.0, 318.0, 319.3, and 321.2 pm,[56] respectively. Taking only these five nearest neighbors into account, we obtain a second moment value of $M_2=20.2\times10^6$ s^{-2}, which is about 80% of the total value of 24.2×10^6 s^{-2} calculated from the entire lattice sum. Therefore, the CN($Q^{(3)}$-Li) values listed in Table II may be overestimated by up to 20%, and corresponding lower-limit values have been included there to account for this possibility. Inspection of Table III indicates further that for the glasses with $x=0.10$ and 0.17 the number of nearest lithium neighbors of $Q^{(3)}$ units extracted from the first minimum of $g_{SiLi}(r)$ and the numerical values of M_2(^{29}Si-^{7}Li) are in excellent agreement with the NMR results. Figure 10 sketches the structural model emerging from our studies. Each nonbridging oxygen atom attached to a $Q^{(3)}$ species interacts with three lithium ions. Assuming a lithium coordination number of four,[9,57] the local oxygen environment for each lithium includes three nonbridging and one bridging oxygen atoms.

TABLE III. $Q^{(n)}$ distribution, M_2 (^{29}Si-^{7}Li) values and coordination numbers CN[$Q^{(3)}$-Li], obtained from MD simulations. The two values for these coordination numbers correspond to two different cutoff radii r_c for the nn shell: (without brackets) first minimum of $g(r)$, i.e. $r_c=r_{min}$; (with brackets) slightly smaller radius such that $g(r_c)=1.1\ g(r_{min})$. The difference of both values is a measure for the uncertainty of the coordination number, resulting from the ambiguity of the definition of the nn shell. The last column lists CN [$Q^{(3)}$-Li] expected for a statistical distribution (using $r_c=r_{min}$).

x	$Q^{(1)}$ (%)	$Q^{(2)}$ (%)	$Q^{(3)}$ (%)	$Q^{(4)}$ (%)	$M_2[Q^{(4)}]$ (10^6 s^{-2})	$M_2(Q^3)$ (10^6 s^{-2})	$M_2[Q^{(2)}]$ (10^6 s^{-2})	r_{SiLi} (±5 pm)	CN [$Q^{(3)}$-Li]	CN (stat) [$Q^{(3)}$-Li]
0.1		2	19	79	4	9.9		318	2.9(2.8)	1.6
0.17		5	33	62	6	12.6	19	321	4.3(3.6)	3.3
0.33	5	22	39	34	15	23	30	312	6.1(5.3)	6.1

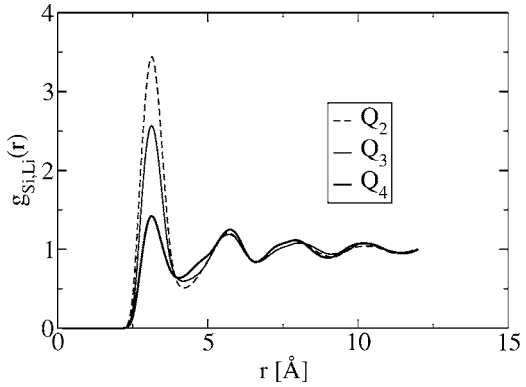

FIG. 7. The partial pair correlation function $g_{Si,Li}(r)$ for different $Q^{(n)}$ units at $x=0.33$.

This arrangement can be perpetuated to form low-dimensional domains in which the lithium ions and the $Q^{(3)}$ units are clustered together, whereas the $Q^{(4)}$ units remain very remote from the Li^+ ions. Altogether, these conclusions are in excellent agreement with a previous structural analysis of lithium disilicate glass based on a neutron diffraction study with $^{6/7}$Li isotopic substitution.[9]

B. The compositional evolution of cluster structure: Discrepancies between NMR and MD results

While NMR and MD simulation are in excellent general agreement regarding the nonstatistical environment of the $Q^{(3)}$ units with lithium ions, conceptually consistent with nanophase segregation for $x<0.33$, a significant discrepancy concerns the lithium environment of the $Q^{(4)}$ units as suggested by the $M_2(^{29}\text{Si-}^7\text{Li})$ analysis: The simulated values are about one order of magnitude larger than the experimental ones, and show an approximately linear concentration dependence, consistent with a statistical distribution of $Q^{(4)}$ relative to Li, even at the lowest lithium content considered ($x=0.10$). In contrast, the NMR data portray significantly weaker $Q^{(4)}$-Li interactions. For example, the experimental value of $M_2=7\times10^5$ s^{-2} for $x=0.15$ implies that basically no lithium ion is in the nn shell of the silicon atom in the $Q^{(4)}$ unit. The reason for this discrepancy can be reasonably well

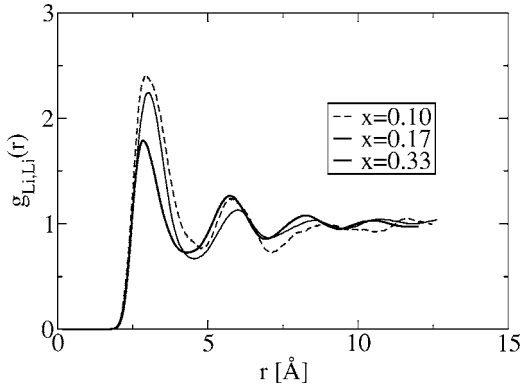

FIG. 8. The partial pair correlation function $g_{Li,Li}(r)$ for different concentrations.

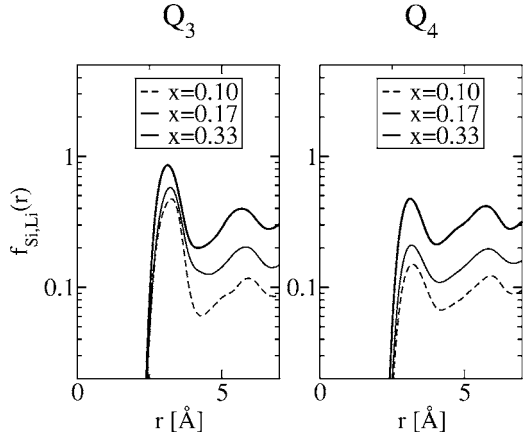

FIG. 9. The scaled pair correlation function $f_{Si,Li}(r)$ for different concentrations for $Q^{(3)}$ units (left) and $Q^{(4)}$ units (right).

understood in terms of the metastable subliquidus immiscibility in the Li_2O-SiO_2 system: For $x=0.1$ and 0.17, the equilibration temperatures implied by the cooling rates in the MD study (1250 K) lie in the vicinity of the critical temperature (1270 K). For this reason, we can expect that the degree of cation segregation in the simulated glasses tends to be less well developed than in the experimental glasses.

The observed superlinear dependence of $M_2(x)$ for the $Q^{(4)}$ units appears curious, at first glance, as the ion distribution in the glass is clearly not homogeneous. Nevertheless, an explanation can be given if one assumes that the segegration phenomenon becomes increasingly more pronounced, as the lithium concentration is lowered. The overall effect observed may then arise from a combination of two effects.

1. *Composition dependent surface/volume ratio of the clusters*. The low-dimensional Li clusters, as indicated in Fig. 10, are characterized by the number density ρ_{cl} and some average individual volume V_{cl}. If we postulate that the size V_{cl} increases with decreasing concentration, then $V_{cl} \propto x^{-\alpha}$ with $\alpha>0$. The surface S_{cl} of these clusters may scale

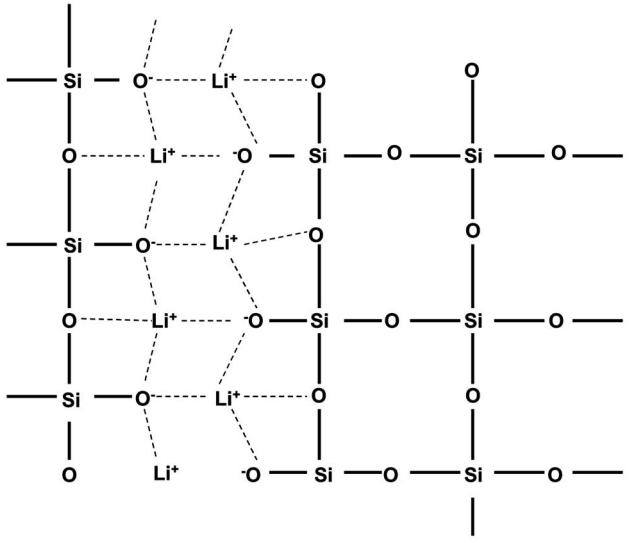

FIG. 10. Schematic depicting the local lithium ion arrangements in segregated lithium silicate glasses.

like $S_{cl} \propto V_{cl}{}^{\beta}$. If the clusters are channels or planes one has $\beta=1$, whereas the case of small spheres is described by $\beta=2/3$. The trivial scaling $V_{cl}\rho_{cl} \propto x$ automatically yields $\rho_{cl} \propto x^{1+\alpha}$. According to Fig. 10 the second moment, representing the closest pairs of silicon atoms in the $Q^{(4)}$ units and lithium ions, may be taken as proportional to the surface of the lithium-rich clusters. This implies $M_2 \propto \rho_{cl} S_{cl} \propto x^{1+\alpha} x^{-\alpha\beta} \propto x^{1+\alpha(1-\beta)}$. Thus, within these model assumptions the superlinear concentration dependence of M_2 is only possible if $\beta<1$ and thus for three-dimensional clusters. This seems to disagree with a coordination number CN($Q^{(3)}$-Li) of 3, which does not allow the construction of three-dimensional clusters. Since, however, the CN values listed in Table III are generally somewhat larger than three, surface effects may have some relevance.

2. *Composition dependent demixing tendency*. One may postulate a nanophase separation into $Li_2Si_2O_5$ glass and a second lithium-poor phase with variable lithium content. For such a model the REDOR response of the $Q^{(3)}$ units will always be dominated by the lithium-rich phase, whereas the REDOR response of the $Q^{(4)}$ units is controlled by the composition of the lithium-poor nanophase. For simplicity, we assume that the lithium ions are statistically distributed in this dilute phase and that their first coordination sphere contains four oxygen atoms. As a result of their low concentration, the majority of the lithium ions will then be isolated, and their first coordination sphere contains no more than a single nonbridging oxygen atom originating from a $Q^{(3)}$ unit. The other three oxygen atoms completing the nearest-neighbor environment are of the bridging type, connecting $Q^{(3)}$ and $Q^{(4)}$ or two $Q^{(4)}$ species. Each such bridging oxygen atom interacting with a Li^+ ion then directs one or two $Q^{(4)}$ silicon atoms within a 320–350 pm distance of the ^{7}Li spins; producing a significant REDOR effect. In reality, we will observe this particular scenario if the extent of nanophase segregation as predicted by the metastable immiscibility curve is not fully realized in the experimental samples studied here. In this case, we will observe a superlinear $M_2(x)$ dependence for the $Q^{(4)}$ units if the extent of nanophase separation achieved decreases with increasing x value. Such an assumption is not improbable, as maximum demixing tendency would be expected in the spinodal decomposition region, which is centered about 10 mol % Li_2O. In contrast, nanophase segregation at compositions outside of the spinodal region may be kinetically inhibited at higher lithia contents, as the bulk composition approaches that of single-phase lithium disilicate glass.

To summarize, the discrepancy observed between NMR and MD results regarding the compositional evolution of $M_2[Q^{(4)}\text{-Li}]$ most likely reflects the different degrees of nanophase segregation portrayed by both methods.

The second evident discrepancy between the NMR and the MD results concerns lithium disilicate glass ($x=0.33$), for which MD indicates that the number of lithium atoms in the nn shell and the second moments of the $Q^{(3)}$ units are substantially higher than suggested by NMR. The MD simulation produces a local $Q^{(3)}$ environment that is very similar to that in crystalline $Li_2Si_2O_5$ (five nearest lithium neighbors, average Si-Li distance of 307.8 pm). As illustrated by Table III, the average number of Li neighbors of a given $Q^{(3)}$ site is close to that expected for a statistical distribution. In contrast, the NMR results reflect a $Q^{(3)}$-Li interaction that appears weaker than in the crystalline compound and also weaker than predicted from the MD study. No good explanation for this effect can be given at the present time. Either the Si-Li distances in the experimental glasses are significantly longer than in the simulated glasses or the topology adopted by the experimental glasses differs significantly from a statistical network. To elucidate the microscopic consequences of the segregation phenomena in lithium silicate computationally in more detail, longer simulations, and, possibly, better force fields for the simulations are required. On the experimental side, a more systematic study of thermally annealed samples would be instructive.

VI. CONCLUSIONS

In summary, the combined NMR and MD results of the present study offer insights into the structural organization of lithium silicate glasses. For the low-lithia region the experimental and simulated structures are in excellent agreement with each other and portray a nanophase-segregated structure with lithium-enriched domains. Based on average $Q^{(3)}$-Li distances (from MD) and second moment values (from NMR), average coordination numbers for the $Q^{(3)}$ units with Li^+ ions have been derived for these domains, leading to the channel-like arrangement proposed in Fig. 10. Significant deviations between NMR and MD results are noted for the structure of the lithium disilicate glass and the details of the $Q^{(4)}$-lithium interactions. The latter discrepancy points consistently into the direction that the clustering tendency portrayed by the MD simulations is not as fully developed as that reflected in the experimental results. We believe that these deviations are related to the large difference (about 300–400 K) between the glass transition temperatures relevant in the computer simulations and those measured experimentally. We speculate that the segregation and domain growth processes resulting in the phase separation of lithium silicate glasses occur in this temperature interval and are therefore not fully reflected in the simulated structures. Finally, the results of the present study indicate that alkali ion clustering is unimportant at glass compositions with higher lithium contents ($x \geqslant 0.33$). This should be borne in mind in the further development and refinement of future approaches modelling ion dynamics and transport in silicate glass-based solid electrolytes.

ACKNOWLEDGMENTS

This work was supported by the Deutsche Forschungsgemeinschaft (SFB 458). H.L. thanks the Fond der Chemischen Industrie. Stimulating discussions with Stefan Puls are gratefully acknowledged.

[1] G. N. Greaves, J. Non-Cryst. Solids **71**, 203 (1985).
[2] G. N. Greaves, S. J. Gurman, C. R. A. Catlow, A. V. Chadwick, S. Houde-Walter, B. Dobson, and C. M. B. Henderson, Philos. Mag. A **64**, 1059 (1991).
[3] L. van Wüllen, B. Gee, L. Züchner, M. Bertmer, and H. Eckert, Ber. Bunsenges. Phys. Chem. **100**, 1539 (1996).
[4] S. Sen and J. F. Stebbins, Phys. Rev. B **50**, 822 (1994).
[5] M. G. Mortuza, R. Dupree, and D. Holland, J. Non-Cryst. Solids **281**, 108 (2001).
[6] L. Olivier, X. Yuan, A. N. Cormack, and C. Jäger, J. Non-Cryst. Solids **293-295**, 53 (2001).
[7] A. Meyer, J. Horbach, W. Kob, F. Kargl, and H. Schober, Phys. Rev. Lett. **93**, 027801 (2001).
[8] A. J. G. Ellison, D. L. Price, J. E. Dickinson, and A. C. Hannon, J. Chem. Phys. **102**, 9647 (1995).
[9] J. Zhao, P. H. Gaskell, M. M. Cluckie, and A. K. Soper, J. Non-Cryst. Solids **232-234**, 721 (1998).
[10] O. V. Mazurin, G. P. Roskova, and E. A. Parai-Koshits, *Phase Separation in Glass* (North Holland, Amsterdam, 1984).
[11] Y. Moriya, D. H. Warrington, and R. W. Douglass, Phys. Chem. Glasses **8**, 19 (1967).
[12] K. Nakagawa and T Izumitanis, Phys. Chem. Glasses **10**, 179 (1969)
[13] M. Tomozawa, Phys. Chem. Glasses **13**, 161 (1972).
[14] R. J. Charles, J. Am. Ceram. Soc. **49**, 55 (1966).
[15] W. Haller, D. H. Blackburn, and J. H. Simmons, J. Am. Ceram. Soc. **587**, 120 (1974).
[16] S. S. Kim and T. H. Sanders, Jr., J. Am. Ceram. Soc. **74**, 1833 (1991).
[17] W. Smith, G. N. Greaves, and M. J. Gillan, J. Non-Cryst. Solids **192-193**, 267 (1995).
[18] C. Huang and A. C. Cormack, J. Chem. Phys. **93**, 8180 (1990).
[19] C. Huang and A. C. Cormack, J. Chem. Phys. **95**, 3634 (1991).
[20] J. Du and A. N. Cormack, J. Non-Cryst. Solids **349**, 66 (2004).
[21] J. Oviedo and J. F. Sanz, Phys. Rev. B **58**, 9047 (1998).
[22] P. Jund, W. Kob, and R. Jullien, Phys. Rev. B **64**, 134303 (2001).
[23] E. Sunyer, P. Jund, W. Kob, and R. Jullien, J. Non-Cryst. Solids **307-310**, 939 (2002).
[24] J. Horbach, W. Kob, and K. Binder, Phys. Rev. Lett. **88**, 125502 (2002).
[25] X. Yuan and A. Cormack, J. Non-Cryst. Solids **283**, 69 (2001).
[26] A. N. Cormack, J. Du, and T. R. Zeitler, Phys. Chem. Chem. Phys. **4**, 3193 (2002).
[27] H. Lammert and A. Heuer, Phys. Rev. B **70**, 024204 (2004).
[28] R. D. Banhatti and A. Heuer, Phys. Chem. Chem. Phys. **3**, 5104 (2001)
[29] R. Dupree, D. Holland, and D. S. Williams, J. Non-Cryst. Solids **81**, 185 (1986).
[30] R. Dupree, D. Holland, and M. G. Mortuza, J. Non-Cryst. Solids **116**, 148 (1990).
[31] S. Sen, C. Gerardin, A. Navrotsky, and J. E. Dickinson, J. Non-Cryst. Solids **168**, 64 (1994).
[32] C. Schramm, B. DeJong, and V. Parziale, J. Am. Chem. Soc. **106**, 4396 (1984).
[33] H. Maekawa, T. Maekawa, K. Kawamura, and T. Yokokawa, J. Non-Cryst. Solids **127**, 53 (1991).
[34] B. H. W. S. DeJong, K. D. Keefer, G. E. Brown, Jr., C. M. Taylor, Geochim. Cosmochim. Acta **45**, 1291 (1981).
[35] H. Eckert, S. Elbers, J. D. Epping, M. Janssen, M. Kalwei, W. Strojek, and U. Voigt, Top. Curr. Chem. **246**, 195 (2004).
[36] J. H. van Vleck, Phys. Rev. **74**, 1168 (1948).
[37] S. J. Gurman, J. Non-Cryst. Solids **125**, 151 (1990).
[38] T. Gullion, Concepts Magn. Reson. **10**, 277 (1998).
[39] J. R. Garbow and T. Gullion, J. Magn. Reson. (1969-1992) **95**, 442 (1991).
[40] M. Bertmer and H. Eckert, Solid State Nucl. Magn. Reson. **15**, 139 (1999).
[41] J. C. C. Chan and H. Eckert, J. Magn. Reson. **147**, 170 (2000).
[42] W. Strojek, M. Kalwei, and H. Eckert, J. Phys. Chem. **108**, 7061 (2004).
[43] A. Schmidt, R. A. McKay, and J. Schaefer, J. Magn. Reson. (1969-1992) **96**, 644 (1992).
[44] C. Hudalla, H. Eckert, and R. Dupree, J. Phys. Chem. **100**, 15896 (1996).
[45] M. Bak, J. T. Rasmussen, and N. C. Nielsen, J. Magn. Reson. **147**, 296 (2000).
[46] B. Gee, and H. Eckert, Solid State Nucl. Magn. Reson. **5**, 113 (1995).
[47] D. Massiot, F. Fayon, M. Capron, I. King, S. Le Calve, B. Alonso, J. O. Durand, B. Bujoli, Z. Gan, and G. Hoatson, Magn. Reson. Chem. **40**, 70 (2000).
[48] J. Habasaki, Mol. Phys. **70**, 513 (1990).
[49] J. Habasaki, I. Okada, and Y. Hiwatari, Mol. Simul. **9**, 319 (1992).
[50] J. Habasaki, I. Okada, and Y. Hiwatari, Mol. Simul. **10**, 19 (1993).
[51] H. Doweidar, J. Non-Cryst. Solids **194**, 155 (1996).
[52] B. A. Maksimov, Y. A. Kharitonov, V. V. Ilyukhin, and N. V. Belov, DANKA **178**, 1309 (1968).
[53] H. Voellenkle, Z. Kristallogr. **154**, 77 (1981).
[54] K. F. Hesse, Acta Crystallogr., Sect. B: Struct. Crystallogr. Cryst. Chem. **33**, 901 (1977).
[55] B. Gee, M. Janssen, and H. Eckert, J. Non-Cryst. Solids **215**, 41 (1997).
[56] B. deJong, P. Slaats, H. Super, N. Veldman, and A. Spek, J. Non-Cryst. Solids **176**, 164 (1994).
[57] Z. Xu and J. F. Stebbins, Solid State Nucl. Magn. Reson. **5**, 103 (1995).